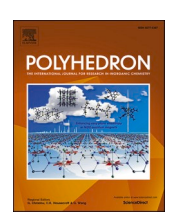
ELSEVIER

Contents lists available at ScienceDirect

# Polyhedron

journal homepage: www.elsevier.com/locate/poly





# Ruthenium terpyridine Phenol-Substituent supports PCET and semiquinone-like behavior

Katherine L. Moffa <sup>a</sup>, Claire N. Teahan <sup>a</sup>, Charlotte L. Montgomery <sup>a</sup>, Samantha L. Shepherd <sup>b</sup>, John C. Dickenson <sup>b</sup>, Kaitlyn R. Benson <sup>a</sup>, Mark Olsen <sup>a</sup>, Walter J. Boyko <sup>a</sup>, Mark Bezpalko <sup>a</sup>, W. Scott Kassel <sup>a</sup>, Timothy J. Dudley <sup>c,\*</sup>, Daniel P. Harrison <sup>b,\*</sup>, Jared J. Paul <sup>a,\*</sup>

- <sup>a</sup> Department of Chemistry, Villanova University, 800 Lancaster Ave., Villanova, PA 19085, United States
- <sup>b</sup> Department of Chemistry, Virginia Military Institute, Department of Chemistry, Lexington, VA 24450, United States
- c Math, Science and Technology Department, University of Minnesota, Crookston, 2900 University Ave., Crookston, MN 56716, United States

#### ARTICLE INFO

#### Keywords: Catalysis Ruthenium Terpyridine Hydroxy-phenyl PCET Semiquinone

#### ABSTRACT

Ligands play a central role in dictating the electronic properties of metal complexes to which they are coordinated. A fundamental understanding of changes in ligand properties can be used as design principles for more efficient catalysts. Designing ligands that have multiple protonation states that will change the properties of the coordination complex would be useful as potential ways of controlling catalysis, for example, as an on/off switch where one redox state exists below thermodynamic potential and another exists above. Thus, phenol moieties built into strongly coordinating ligands, like that of tpyPhOH (4'-(4-hydroxyphenyl)-2,2':6',2''-terpyridine) may provide such a handle. Herein, we report the electrochemical and spectral characterization, and the crystallographic and computational analysis of two ruthenium analogs: [Ru(tpy)(tpyPhOH)](PF<sub>6</sub>)<sub>2</sub> and [Ru(tpyPhOH)<sub>2</sub>]  $(PF_6)_2$  (tpy = 2,2':6',2''-terpyridine). Cyclic voltammetry and differential pulse voltammetry indicate that two redox events occur, one of which is pH independent and we hypothesize that these follow an electrochemicalchemical-electrochemical (ECE) mechanism. XRD results of the ruthenium complexes' protonated forms are generally consistent with expected bond lengths and angles and are in agreement with computational modeling. The properties are compared to a previously reported analog that contains the -OH group directly connected to terpyridine, [Ru(tpyOH)<sub>2</sub>](PF<sub>6</sub>)<sub>2</sub>, where tpyOH is 4'-hydroxy-2,2':6',2''-terpyridine, with some intriguing differences. Overall, these data indicate that the phenyl-substituent decouples the phenol such that it behaves both as an electron withdrawing substituent and a location for a ligand centered oxidation event to occur.

### 1. Introduction

Electron transfer reactions are often found coupled with acid/base chemistry, facilitating the electron transfer process. This class of coupled reactions is well studied and commonly referred to as Proton Coupled Electron Transfer (PCET) [1–9]. A critical component of these reactions involves the transfer of protons along with electrons. Studying the details of PCET in different systems can play a significant role in guiding the development of catalysts for several reactions of interest, such as water oxidation, carbon dioxide reduction, and nitrogen fixation. Metal complexes are often studied as catalysts because they have the ability to mediate electron transfer reactions and overcome the high activation energies of complex reactions [10,11]. Incorporating protonatable ligands into metal complexes presumably alters their electron transfer

properties. Furthermore, a change in proton content could provide a way for tuning electron transfer reactions by altering overall metal complex charges and/or oxidation state, possibly resulting in a catalytic on/off switch [12–22]. To further develop an understanding of how and to what extent various protonation states influence the electrochemical, structural, and electronic properties of metal complexes, a set of ruthenium-based terpyridine complexes were synthesized and characterized via UV–visible spectroscopy and electrochemistry. Computational analysis was utilized to provide additional insight into the experimental results.

Our laboratory is interested in studying how altering protonation states of ligands with hydroxyl-substitutions affects the structural and electronic properties of ruthenium polypyridyl complexes [23–27]. The changes in protonation state can alter catalytic activity in water

E-mail addresses: timothy.j.dudley@gmail.com (T.J. Dudley), harrisondp@vmi.edu (D.P. Harrison), jared.paul@villanova.edu (J.J. Paul).

<sup>\*</sup> Corresponding authors.

oxidation catalysis and change photodissociation, which has been linked to anti-cancer activity [28–31]. Most notably, substitutions in the 4,4′-and 6,6′-positions of the polypyridyl ring structure have dramatic effects upon the Ru³+/2+ oxidation state. There is a systematic shift to lower redox potentials as the number of hydroxyl groups in tris-bipyridyl complexes increases. This shift is a result of the ligands becoming more electron-donating, stabilizing the higher 3<sup>+</sup> oxidation state [32]. Upon deprotonation of hydroxyl groups in the 4- and 6- positions, further electron-donation to the metal center is observed and can be visualized by resonance structures. This additional electron-donating character upon deprotonation decreases the reduction potential of the Ru³+/2+ to an even greater extent. Impressively, the most significant change to date is observed upon deprotonation of [Ru<sup>II</sup>(bpy(OH)<sub>2</sub>)<sub>3</sub>]<sup>2+</sup> to [Ru<sup>II</sup>(bpy(O')<sub>2</sub>)<sub>3</sub>]<sup>4-</sup> of nearly a 1.5 V decrease (e.g.  $\Delta E_{1/2}(Ru^{III/II}) = -1.43$  V) in the reduction potential [25].

Previous reports from our group reported incorporating hydroxysubstitutions into ruthenium terpyridine complexes, utilizing the 4'-hydroxy-2,2':6',2''-terpyridine (tpyOH) ligand [24]. In these complexes, the hydroxy- group is directly attached to the central pyridine ring and trans to the coordinating nitrogen. With all of our previous work focusing on direct attachment of hydroxy-moieties to the pyridine ring, we sought to learn how furthering the spacing of the hydroxy- group from the pyridine ring impacts the electronic and structural properties of this class of complexes. Here, we further extend our work and report homoleptic and heteroleptic complexes containing the 4'-(4-hydroxyphenyl)-2,2':6',2''-terpyridine (tpyPhOH) ligand, where the hydroxyl group is part of a phenyl ring attached to the central terpyridine ring, Fig. 1. While the hydroxyl group is still in electronic communication with the metal center, we anticipated that this phenyl spacer will have a diminished influence on the metal center, considering the necessary dihedral twisting of the ring with respect to the terpyridine portion of the ligand [33]. Herein, we report a systematic evaluation of the structural and electronic properties of ruthenium complexes containing the tpyPhOH ligand as a consequence of changing ligand protonation states.

#### 2. Experimental

#### 2.1. General procedures

All chemicals were purchased from Oakwood Chemical Company unless otherwise stated. RuCl $_3$ -3H $_2$ O was purchased from Pressure Chemical Company. Ethanol was purchased from Pharmco. Methanol, acetonitrile, and acetone were purchased from Fischer Chemical. [Ru (tpy)Cl $_3$ ] was synthesized according to previously published methods [34]. For studies done in aqueous solutions, all ruthenium hexafluorophosphate salts were converted to chloride salts by precipitation from acetone using tetrabutylammonium chloride (TBACl) dissolved in acetone. All other studies in nonaqueous solutions were carried out

utilizing the ruthenium hexafluorophosphate salts. Elemental analysis for ruthenium complexes were carried out by Atlantic Microlabs Inc., Norcross GA. Aqueous solutions were prepared using a Millipore DirectQ UV water purification system. Infrared spectroscopy was performed using a Perkin Elmer Two Fourier Transform infrared spectrometer with an ATR accessory. Electrochemical experiments were performed using a Pine Research WaveNow Wireless Potentiostat. UV/ Visible spectroscopy was carried out using an Agilent Technologies Cary Series UV-Vis-NIR Spectrophotometer. pH measurements were made with an Oakton pH 2700 pH meter. <sup>1</sup>H NMR scans were collected on a Varian 300 MHz Fourier Transform NMR Spectrometer or a JEOL ECZ500R 500 MHz Fourier Transform NMR Spectrometer. Mass spectrometry data was collected using an AID Sciex Triple TOF 5600 + with a liquid chromatography and electrospray ionization (ESI) method outlined in the supporting information. Mass differences are reported for the most intense peak in the isotopic window for the ruthenium complexes.

#### 2.2. Synthesis of tpyPhOH

4'-(4-hydroxyphenyl)-2,2':6',2''-terpyridine, tpyPhOH, was synthesized on multi-gram scale according to literature procedure [35]. Briefly, HBr (48%) was added to an off-white 4'-(4-methoxyphenyl)-2,2':6',2''-terpyridine [33] to produce a homogeneous orange solution that precipitated a bright orange solid after several hours of refluxing. The reaction was neutralized after 24 h by the addition of NaOH pellets, where the orange solid turned into a fine, pale-green precipitate that was collected via medium porosity fritted funnels and rinsed with ethanol. The material was recrystallized from ethanol prior to use. Characterization data is consistent with previous reports.  $^1$ H NMR (400 MHz, DMSO- $D_6$ )  $\delta$  8.76 (dd, J = 4.8, 1.7 Hz, 2H), 8.66 (m, 4H), 8.03 (td, J = 7.7, 1.9 Hz, 2H), 7.79 (d, J = 8.6 Hz, 2H), 7.52 (dd, J = 7.6, 4.7 Hz, 2H), 6.97 (m, 2H).

#### 2.3. Synthesis of [Ru(tpyPhOH)Cl<sub>3</sub>]

The synthesis of [Ru(tpyPhOH)Cl $_3$ ] was modelled after the literature preparation of [Ru(tpy)Cl $_3$ ] [34]. A 0.26 g (1.0 mmol) sample of RuCl $_3$ ·3H $_2$ O and 0.325 g (1.0 mmol) sample of tpyPhOH was added to a round-bottom flask containing 125 mL of ethanol. The reaction flask was heated to 80 °C for 3 h with vigorous stirring under reflux. After the reaction was completed, the solution was cooled to room temperature. The precipitated black complex was filtered and washed with ethanol, then ether and used directly in the next synthetic procedures. Yield: 0.45 g (0.76 mmol), 76%.

#### 2.4. Synthesis of [Ru(tpy)(tpyPhOH)](PF<sub>6</sub>)<sub>2</sub>

A round-bottom flask containing 40 mL of ethanol was degassed with

Fig. 1. Ruthenium complexes and varying protonation states containing the tpyPhOH ligand reported in this work.

argon for 30 min. A 0.35 g (0.79 mmol) sample of  $[Ru(tpy)Cl_3]$  and 1.5 mL trimethylamine was added to the flask. The solution was heated to 80 °C to reflux for 2 h. After the reaction was completed, the solution was filtered hot to collect the purple solid,  $[Ru(tpy)(Cl)]_2(\mu-Cl)_2]$ . The solid was rinsed with ethanol, then ether and 0.28 g (0.34 mmol) of solid was collected to be used directly in the next step. <sup>1</sup>H NMR characterization was consistent with previous reports, Figure S6 [36].

A round-bottom flask containing 60 mL 1:1 ethanol:water was degassed with argon for 30 min. To the flask, 0.28 g (0.34 mmol) [{Ru  $(tpy)(Cl)_2(\mu-Cl)_2$  and 0.22 g (0.68 mmol) 4'-(4-hydroxyphenyl)-2, 2':6', 2''-terpyridine (tpyPhOH) were added. The reaction mixture was heated to 80  $^{\circ}$ C for 2 h. After the reaction was complete, the solution was cooled to room temperature and filtered to remove any insoluble materials. Distilled water was added to dilute the solution and 8 drops of concentrated HCl were added to ensure protonation of the complex. An excess of NH<sub>4</sub>PF<sub>6</sub> in H<sub>2</sub>O was added to precipitate the red complex. The solid was filtered and washed with water, then ether to yield product. Yield: 0.52 g (0.55 mmol) 81%.  $^{1}$ H NMR (300 MHz, CD<sub>3</sub>CN): δ 9.0 (s, 2H), 8.8(d, 2H), 8.7 (d, 2H), 8.5 (d, 2H), 8.4 (t, 1H), 8.1 (d, 2H), 8.0-7.9 (m, 4H), 7.5 (d, 2H), 7.4 (d, 2H), 7.2-7.1 (m, 6H). Anal. Calc. for RuC<sub>36</sub>N<sub>6</sub>O<sub>1</sub>H<sub>26</sub>P<sub>2</sub>F<sub>12</sub>·4H<sub>2</sub>O: C, 42.32; N, 8.23; H, 3.35. Found: C, 42.43; N, 8.52; H, 2.82%. ESI-MS: Found 330.0612 Da (M)<sup>+2</sup>, Calculated  $330.0606 \text{ Da (M)}^{+2}$ , mass difference 1.82 ppm.

#### 2.5. Synthesis of [Ru(tpyPhOH)<sub>2</sub>](PF<sub>6</sub>)<sub>2</sub>

For 30 min, 30 mL of 1:1 ethanol:water was degassed with argon. Following degassing, 0.44 g (0.83 mmol) of previously synthesized [Ru (tpyPhOH)Cl<sub>3</sub>] and 1.5 mL of triethylamine were added and heated at 80 °C under argon for 2 h. The solution was then cooled to room temperature and filtered with a fritted funnel. The solid was washed with ethanol and then ether and allowed to air dry. The mass of the resulting solid, which we hypothesize to be the chloro bridged dimer of tpyPhOH akin to [{Ru(tpy)(Cl)}<sub>2</sub>( $\mu$ -Cl)<sub>2</sub>], was 0.22 g (0.22 mmol) [36].

Following this step, 60 mL of 1:1 ethanol:water was degassed with argon for 30 min. Following degassing, 0.22 g (0.22 mmol) of the solid and 0.14 g (0.44 mmol) of the tpyPhOH ligand were added. The reaction was heated at 80 °C under argon for two hours. The solution was cooled to room temperature and filtered using a Buchner funnel to remove any unreacted ligand. The filtrate was diluted with water and HCl was added. NH<sub>4</sub>PF<sub>6</sub> was dissolved in water and added to the filtrate to precipitate the PF<sub>6</sub> salt. The solid was filtered and washed with water, then ether to yield product. Yield: 0.16 g (0.16 mmol) 69%.  $^{1}$ H NMR (300 MHz, CD<sub>3</sub>CN):  $\delta$  9.0 (s, 4H), 8.6(d, 4H), 8.1 (d, 4H), 7.9 (dd, 4H), 7.4 (d, 4H), 7.2 (m, 8H). Anal. Calc. for RuC<sub>42</sub>N<sub>6</sub>O<sub>2</sub>H<sub>30</sub>P<sub>2</sub>F<sub>12</sub>·0.5H<sub>2</sub>O: C, 48.01; N, 8.00; H, 2.97. Found: C, 47.92; N, 8.16; H, 3.16%. ESI-MS: Found 376.0744 Da (M)<sup>+2</sup>, Calculated 376.0737 Da (M)<sup>+2</sup>, mass difference 1.86 ppm.

#### 2.6. X-ray data collection

[Ru(tpyPhOH)<sub>2</sub>](PF<sub>6</sub>)<sub>2</sub>. Crystals of [Ru(tpyPhOH)<sub>2</sub>](PF<sub>6</sub>)<sub>2</sub> were grown by diffusion of ether into a solution of the complex dissolved in acetonitrile. X-Ray data on a crystal were collected on a Bruker-AXS Kappa Apex II CCD diffractometer with 0.71073 Å Mo Kα radiation. All diffractometer manipulations, including data collection, integration, scaling, and absorption corrections were carried out using the Bruker Apex2 software [37]. The structure was solved using Sir92 [38], and refined (full-matrix-least squares) using the Oxford University Crystals for Windows program [39,40]. The final CIF is available as supporting material.

 $[Ru(tpy)(tpyPhOH)](PF_6)_2$ . Crystals of  $[Ru(tpy)(tpyPhOH)](PF_6)_2$  were grown by the slow diffusion of ether into an acetonitrile solution of the complex. X-Ray Crystallography for  $[Ru(tpy)(tpyPhOH)](PF_6)_2$  was performed on a Rigaku Corporation XtaLAB mini (ROW) at 170 K with an Oxford Cryosystems Cryostream 800 and accompanying Oxford

AD61 Dry Air Unit, processed with CrysAlisPro, and solved with ShelX using Olex2 1.3 [41,42].

#### 2.7. Cyclic voltammetry

Cyclic voltammetry measurements were performed on a Pine Research Wavenow wireless potentiostat. Typical concentrations for metal complexes ranged from 1.0 to 3.0 mM. A standard three electrode setup was used for all studies. For studies carried out in acetonitrile a Ag/Ag<sup>+</sup> reference electrode filled with 0.1 M tetrabutylammonium hexafluorophosphate (TBAPF<sub>6</sub>), platinum wire auxiliary electrode, and a glassy carbon working electrode was used. All complexes were prepared in 0.1 M TBAPF<sub>6</sub> supporting electrolyte solution. Ferrocene (Fc) was used as an internal standard and all data is reported versus the Fc<sup>+/</sup> <sup>0</sup> couple. For studies carried out in aqueous solution, a three-electrode setup with an Ag/AgCl reference electrode containing 3 M KCl, platinum wire auxiliary electrode, and glassy carbon working electrode was used. Complexes were prepared using the Britton-Robinson buffer system and the pH was checked after the complex was dissolved. In all studies, the solutions were degassed for approximately 20 min with argon prior to data collection, and the glassy carbon electrode was polished before each scan.

#### 2.8. Differential pulse voltammetry

Differential pulse voltammetry (DPV) measurements were performed on a Pine Research WaveNow Wireless potentiostat. The typical concentration for metal complexes was 3.0 mM. A three-electrode setup with an Ag/AgCl reference electrode containing 3 M KCl, platinum wire auxiliary electrode, and glassy carbon working electrode was used. [Ru (tpy)(tpyPhOH)]Cl<sub>2</sub> solutions were prepared using the Britton-Robinson buffer system containing 5% DMSO and the pH was checked after the complex was dissolved. The addition of 0.2 M sodium hydroxide was used once the metal complex was added to alter the pH. In all studies, the glassy carbon electrode was polished before each scan. General DPV parameters: a period of 100 ms, width of 10 ms, height of 50 mV, and potential increment of 10 mV.

#### 2.9. Buffer system for electrochemical pH studies

pH measurements were carried out using an Oakton pH 2700 pH meter, utilizing a three-point calibration at pH = 4, 7, and 10. Britton-Robinson buffer solutions were made from a stock solution of 0.04 M acetic acid, 0.04 M boric acid, and 0.04 M phosphoric acid. The addition of 0.2 M sodium hydroxide was used once the metal complex was added to correct the pH.

#### 2.10. UV/Visible spectroscopy

UV/Visible spectroscopic measurements were collected on an Agilent Technologies Cary Series UV–Vis-NIR Spectrophotometer. For aqueous studies, enough 1.0 mM stock solution consisting of complex dissolved in DMSO was added to buffer solutions to afford a sample containing 5% DMSO. Buffers were prepared using solutions referenced from the Chemical Technicians' Ready Reference Handbook [43]. Each buffer was checked for pH accuracy. If its pH was>0.20 pH units from the desired pH, concentrated HCl or NaOH was used to correct it. The buffer solutions ranged from pH 1.0 to 13.0 in half-pH unit increments. For nonaqueous studies, spectroscopic grade methanol (MeOH), ethanol (EtOH), acetonitrile (MeCN), and acetone were used with 5% DMSO added to aid in solubility. Data was collected in pure solvent along with added 0.1 M HPF<sub>6</sub> to ensure protonation and added 0.1 M tetrabuty-lammonium hydroxide (TBAOH) to obtain spectra of the deprotonated form of the complex.

#### 2.11. Computational studies

All computations were performed using Gaussian09 with default parameters unless otherwise specified [44]. Geometries were optimized at the M06-L level utilizing the LANL2DZ basis set for Ru and the 6-31G\* basis set for all other atoms. Open-shell calculations utilized an unrestricted formalism for representing the wavefunction. Frequencies were calculated at each minimum using analytic second derivatives and each were determined to have zero imaginary modes. Vertical transitions were calculated using time-dependent DFT, utilizing the same method and basis sets as for ground state calculations. All ground and excited state calculations included solvent effects through use of the polarizable continuum model (CPCM) with water as the solvent.

#### 3. Results and discussion

# 3.1. Crystal structures of $[Ru(tyPhOH)_2](PF_6)_2$ and $[Ru(tyPhOH)_2](PF_6)_2$

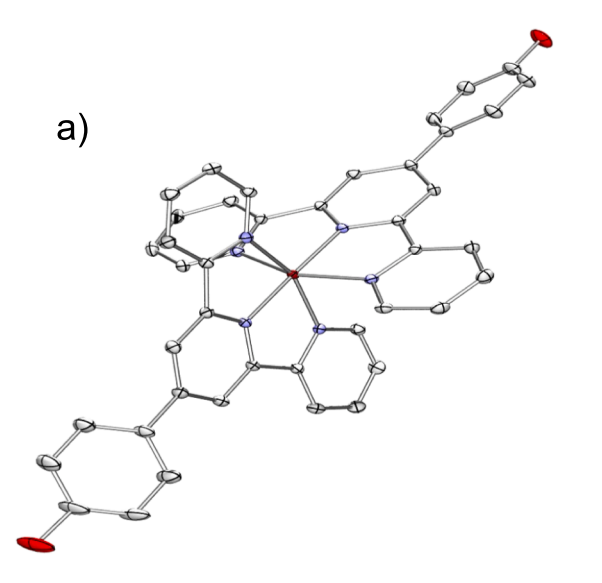
Crystals of both [Ru(tpyPhOH)<sub>2</sub>](PF<sub>6</sub>)<sub>2</sub> and [Ru(tpy)(tpyPhOH)] (PF<sub>6</sub>)<sub>2</sub> were grown by slow diffusion of ether into a solution of the complex dissolved in acetonitrile, Fig. 2. Relevant bond lengths and angles of both complexes are reported in Table 1. Both complexes have a distorted octahedral shape about the Ru center. In addition, for each terpyridine-substituted complex, the central pyridine rings Ru-N bonds are approximately 0.1 Å longer than the Ru-N bonds from the outer pyridine rings, which is commonly observed with Ru-terpyridyl complexes [45,46]. The C—O bond lengths from the phenol portion of the complex are 1.369(3) and 1.364(3) Å in [Ru(tpyPhOH)<sub>2</sub>](PF<sub>6</sub>)<sub>2</sub> and 1.371(4) Å [Ru(tpy)(tpyPhOH)](PF<sub>6</sub>)<sub>2</sub>. These bond lengths are slightly longer (>0.02 Å), compared to polypyridyl complexes where the hydroxyl group is directly attached to the pyridine ring [23,25,46]. This is unsurprising as the electronic effects between the metal and hydroxyl group would decrease when further separated by a phenyl group that is twisted and with disrupting conjugation. The N-Ru-N bond angles are all similar to those reported for other ruthenium terpyridyl complexes

The free tpyPhOH ligand has been crystallized twice previously in work by Darabi et al. and Zhou et al. [47,48]. The ligand has a nearly planar geometry, where the dihedral angle of the phenol ring to the

Table 1 Selected bond distances and angles of  $[Ru(tpyPhOH)_2](PF_6)_2$  and  $[Ru(tpy)(tpyPhOH)](PF_6)_2$ .

Bond Lengths (Å)	[Ru(tpyPhOH) <sub>2</sub> ] (PF <sub>6</sub> ) <sub>2</sub>	[Ru(tpy)(tpyPhOH)] (PF <sub>6</sub> ) <sub>2</sub>
Ru-N1	2.0749(17)	2.078(3)
Ru-N2	1.9829(16)	1.989(3)
Ru-N3	2.0818(17)	2.074(3)
Ru-N4	2.0670(17)	2.069(3)
Ru-N5	1.9805(16)	1.983(3)
Ru-N6	2.0620(17)	2.062(3)
C12-O1	1.369(3)	1.371(4)
C33-O2	1.364(3)	_
Bond Angles (°)		
N1-Ru-N2	79.12(7)	79.05(12)
N1-Ru-N3	157.75(7)	157.75(12)
N1-Ru-N4	94.20(7)	96.15(14)
N1-Ru-N5	98.94(7)	101.43(12)
N1-Ru-N6	89.48(7)	88.60(13)
C7-C8-C9-C10 dihedral O1	22.5(3)	36.2(6)
C28-C29-C30-C31 dihedral O2	31.2(3)	-

central pyridine ring is 6.29° and 6.39°, for the two structures. When complexed to Pd in the square planar [Pd(tpyPhOH)Cl]<sup>+</sup> complex, the dihedral angle increases slightly to  $8.2^{\circ}$  and there are no clear  $\pi$  interactions in the crystal packing [47]. In the [Ru(tpyPhOH)<sub>2</sub>]<sup>2+</sup> complex, both of these dihedral angles increase significantly with angles of 22.52° and 31.19° and increase even more to 36.23° in [Ru(tpy) (tpyPhOH)]<sup>2+</sup>. These large twists relative to the other structures may have to do with the overall crystal packing. In [Ru(tpyPhOH)<sub>2</sub>]<sup>2+</sup> the phenolic portions of the ring system between two separate complexes have a centroid-to-centroid distance of 3.984 Å, which is slightly larger than the typically defined 3.3 to 3.8 Å distance associated with a  $\pi$ - $\pi$ interaction [49]. Nonetheless, this interaction and the steric effects that are not observed with the square planar Pd complexes would help to explain the twist between the central pyridine and phenol portions of the ligand. For the mixed ligand complex,  $[Ru(tpy)(tpyPhOH)]^{2+}$ , the phenolic portion of the ring has a centroid-to-centroid distance with one of the outer rings of another tpyPhOH ligand of 3.816 Å. In work carried out by Iranmanesh et al, two different ruthenium complexes containing



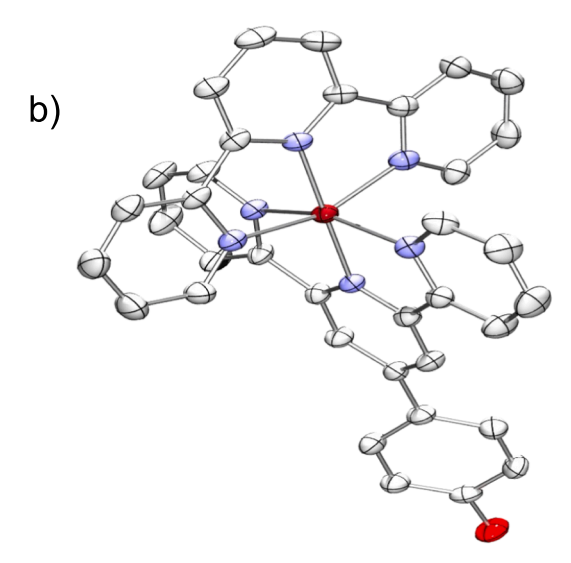


Fig. 2. X-Ray Crystal structures at the 50% ellipsoid probability level of a)  $[Ru(tpyPhOH)_2](PF_6)_2$  and b)  $[Ru(tpy)(tpyPhOH)](PF_6)_2$ . All  $PF_6$  counter ions and hydrogen atoms are omitted for clarity.

a single tpyPhOH ligand are reported [50]. These complexes contain a second terpyridine with a 4'-pyridine substitution and have dihedral angles of 14.26° and 3.30° between the phenolic ring and central pyridine. Interestingly, the phenolic portion of the ring has a centroid-tocentroid distance of 3.887 Å and 3.727 Å, in the packing of these complexes. In these two cases, the phenolic ring aligns with one of the outer pyridine rings of another tpyPhOH ligand, similar to what we observe for the mixed ligand [Ru(tpy)(tpyPhOH)]<sup>2+</sup> complex. This further supports that the packing and twist angle is influenced by  $\pi$  interactions in the crystal lattice. In work carried out by McMurtrie and Dance, the phenyl groups attached to the central pyridine ring in [Ru(tpyPh)<sub>2</sub>]<sup>2+</sup> (tpyPh = 4'-phenyl-2,2':6',2''-terpyridine) are twisted, giving an edge-toface interaction between phenyl rings of different ligands, as opposed to the  $\pi$ - $\pi$  interaction we observe in both [Ru(tpyPhOH)<sub>2</sub>]<sup>2+</sup> and [Ru(tpy) (tpyPhOH)]<sup>2+</sup> [51]. The packing in [Ru(tpyPh)<sub>2</sub>]<sup>2+</sup> gives a dihedral angle of the central pyridine ring to phenyl group of over 30° [51,52].

# 3.2. Computational structures of and $[Ru(tpyPhOH)_2]^{2+}$ (1<sup>2+</sup>) and $[Ru(tpy)(tpyPhOH)]^{2+}$ (2<sup>2+</sup>) in different protonation states

Computational analysis of the tpyPhOH ligand and complexes [Ru  $(tpyPhOH)_2]^{2+}$  (1<sup>2+</sup>) and  $[Ru(tpy)(tpyPhOH)]^{2+}$  (2<sup>2+</sup>) in their varying protonation states were carried out using water as the PCM solvent. Relevant bond lengths and angles are reported in Table 2. All of the complexes studied take on a distorted octahedral shape common for ruthenium polypyridyl complexes despite being necessarily free of other ligand and complex (e.g.  $\pi$ -intermolecular) interactions observed in the crystal packing structure. For  $[Ru(tpyPhOH)_2]^{2+}$ , all of the Ru-N bond distances are slightly longer by approximately 2% in the computational studies compared to the actual crystal structures, which is commonly observed in this type of analysis [53]. Notably, the trend of the central pyridine ring having a shortened bond distance by approximately 0.1 Å compared to the outer pyridine rings is observed in all structures and in line with what is observed for the corresponding crystal structures. The C-O bond lengths of the protonated hydroxyl groups are 1.354 Å and 1.353 Å for complexes  $1^{2+}$  and  $2^{2+}$ , respectively. The bond lengths are indicative of single bonds and compare well with the protonated crystal structures, vide supra. Upon deprotonation, the C-O bond lengths decrease to 1.262 Å and 1.261 Å for complexes  $\mathbf{1}^0$  and  $\mathbf{2}^+$ , respectively. This significant decrease in bond length is indicative of a more double bond character, which can be explained by resonance that results from deprotonation, Fig. 3. This shortening of the C-O length upon deprotonation has been observed previously in both crystal and computational structure analysis for a series of hydroxy-substituted polypyridyl

 Table 2

 Selected computational bond lengths and angles for ruthenium complexes.

Bond lengths (Å)	12+	1+	10	<b>2</b> <sup>2+</sup>	<b>2</b> <sup>+</sup>
Ru-N1	2.117	2.115	2.117	2.116	2.119
Ru-N2	2.007	2.002	2.009	2.009	2.017
Ru-N3	2.117	2.115	2.117	2.117	2.119
Ru-N4	2.117	2.121	2.117	2.115	2.112
Ru-N5	2.007	2.106	2.009	2.007	2.003
Ru-N6	2.117	2.120	2.117	2.114	2.111
C12-O1	1.354	1.354	1.262	1.353	1.261
C33-O2	1.354	1.262	1.262	_	-
Bond Angles (°)					
N1-Ru-N2	78.02	78.19	77.81	77.99	77.60
N1-Ru-N3	156.03	156.37	155.63	156.01	155.17
N1-Ru-N4	92.45	92.50	92.52	92.29	92.43
N1-Ru-N5	101.98	101.91	102.09	102.33	102.30
N1-Ru-N6	92.48	92.54	92.59	92.40	92.53
C7-C8-C9-C10 dihedral	26.89	28.11	13.52	28.30	14.20
01					
C28-C29-C30-C31	26.63	14.30	13.52	-	-
dihedral O2					

ligands, where the substitution is ortho or para to the nitrogen atoms in the polypyridyl ring [23,25].

For  $1^{2+}$ , both phenol ring to central pyridyl rings are twisted with respect to each other, resulting in calculated dihedral angles of  $26.89^{\circ}$  and  $26.63^{\circ}$ . These angles are the average of the two corresponding dihedral angles in the crystal structure that vary significantly from each other ( $22.5^{\circ}$  and  $31.2^{\circ}$ ). The single phenol complex,  $2^{2+}$  has a calculated dihedral angle of  $28.30^{\circ}$ , which is significantly smaller than that of the corresponding crystal structure ( $36.2^{\circ}$ ), further supporting that crystal packing and intermolecular interactions play a significant role in twisting of the ring system, but also indicating some phenyl-tpy ring MO communication. Upon deprotonation of both complexes, the dihedral angle decreases significantly to  $13.52^{\circ}$  for the doubly deprotonated  $1^{0}$  complex and  $14.20^{\circ}$  for the deprotonated  $2^{+}$  complex; upon deprotonation significant resonance mixing in the central pyridyl and phenoxyl ring that will drive planarization, which is also indicated by the shortening of the C—O bond lengths upon deprotonation, *vide supra*.

## 3.3. UV/Visible spectroscopy

All spectroscopy solutions were prepared with 5% DMSO as a result of the low solubility of  $[Ru(tpyPhOH)_2]^{2+}$  in investigated solvents. All of the  $[Ru(tpy)(tpyPhOH)]^{2+}$  complexes were also prepared with 5% DMSO to maintain a consistent analysis.  $[Ru(tpy)(tpyPhOH)]^{2+}$  complexes were also prepared and analyzed to ensure that the DMSO did not have a major impact on peak shifts (See supporting information), even considering their full solubility in aqueous solutions.

A standard pH titration of 4 mM [Ru(tpy)(tpyPhOH)]<sup>2+</sup> with 0.01 M NaOH gave a pK<sub>a</sub> value of 8.61  $\pm$  0.03. Unfortunately, we were unable to carry a standard acid/base titration with [Ru(tpyPhOH)<sub>2</sub>]<sup>2+</sup> due to its poor solubility. However, the calculated pKa value [54] for [Ru(tpy)  $(tpyPhOH)]^{2+}$  is 9.0  $\pm$  0.4 and for  $[Ru(tpyPhOH)_2]^{2+}$  is 8.9  $\pm$  0.7, determined spectrophotometrically by preparing buffered solutions of known Ru concentration, Fig. 4. It is noted that only a single average  $pK_a$ has been determined for the [Ru(tpyPhOH)<sub>2</sub>]<sup>2+</sup> complex, despite containing two deprotonatable hydroxy groups, which is a phenomenon that we have observed for Ru-polypyridyl complexes with hydroxysubstitutions in the pyridyl ring where subsequent deprotonation events cannot be parsed out. The pKa values of the tpyPhOH complexes, result in a slightly more acidic proton than a typical phenol  $pK_a = 9.98$ , indicating that coordination to ruthenium does moderately impact that acid/base properties of the hydroxyl group [55]. However, in the corresponding complexes,  $[Ru(tpy)(tpyOH)]^{2+}$  (pK<sub>a</sub> = 5.85) and [Ru $(tpyOH)_2$ <sup>2+</sup>  $(pK_a = 5.78)$ , the hydroxy-group directly attached to the 4position of the terpyridine ring results in a significantly more acidic proton when compared to an analogous compound of 4-hydroxy-pyridine  $(pK_a = 11.12)$  [24,56,57].

Each complex was studied in five different solvents (water, methanol, ethanol, acetonitrile, and acetone), Fig. 5. The solvents were chosen for solubility of the complexes, varying dielectric constants, and hydrogen bonding ability. The lowest energy  $\lambda_{max}$  for these complexes are reported in Table 3. In the protonated form of [Ru(tpy) (tpyPhOH)]<sup>2+</sup>, all of the  $\lambda_{max}$  values are within 3 nm of each other, ranging from 483 nm to 486 nm. The narrow range holds true for the doubly protonated [Ru(tpyPhOH)<sub>2</sub>]<sup>2+</sup> complexes that have  $\lambda_{max}$  values ranging from 493 to 496 nm. Although subtle, the  $\lambda_{max}$  red shift for these complexes is attributable to a lower dielectric effect. These small solvatochromatic shifts have been observed in other Ru-polypyridyl complexes, including [Ru(tpy)<sub>3</sub>]<sup>2+</sup>, which red shifts 3 nm when changing the solvent from water to methylene chloride [58]. The extra tpyPhOH ligand in [Ru(tpyPhOH)<sub>2</sub>]<sup>2+</sup> results in an approximately 10 nm red shift compared to the mixed ligand [Ru(tpy)(tpyPhOH)]<sup>2+</sup> complex.

More significant peak shifts are observed in the deprotonated forms of the complexes where the  $\lambda_{max}$  values change as a function of two factors: (1) the dielectric constant and (2) the hydrogen bonding ability of the solvent. The lower the dielectric constant of the solvent the larger

Fig. 3.T. tpyPhOH ligand and resonance structures after deprotonation to tpyPhO.

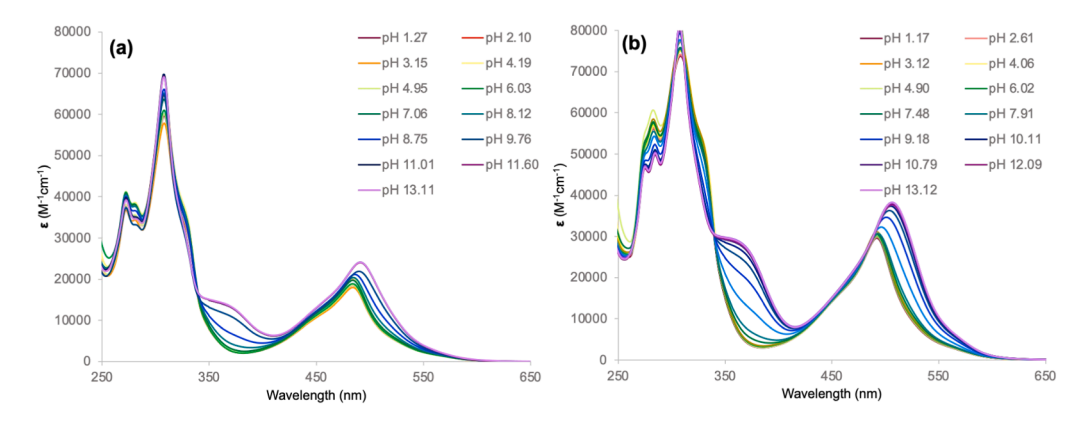


Fig. 4. UV/Visible spectra of (a) 20 µM [Ru(tpy)(tpyPhOH)]Cl<sub>2</sub> and (b) 20 µM [Ru(tpyPhOH)<sub>2</sub>]Cl<sub>2</sub> in aqueous buffers[43] and 5% DMSO.

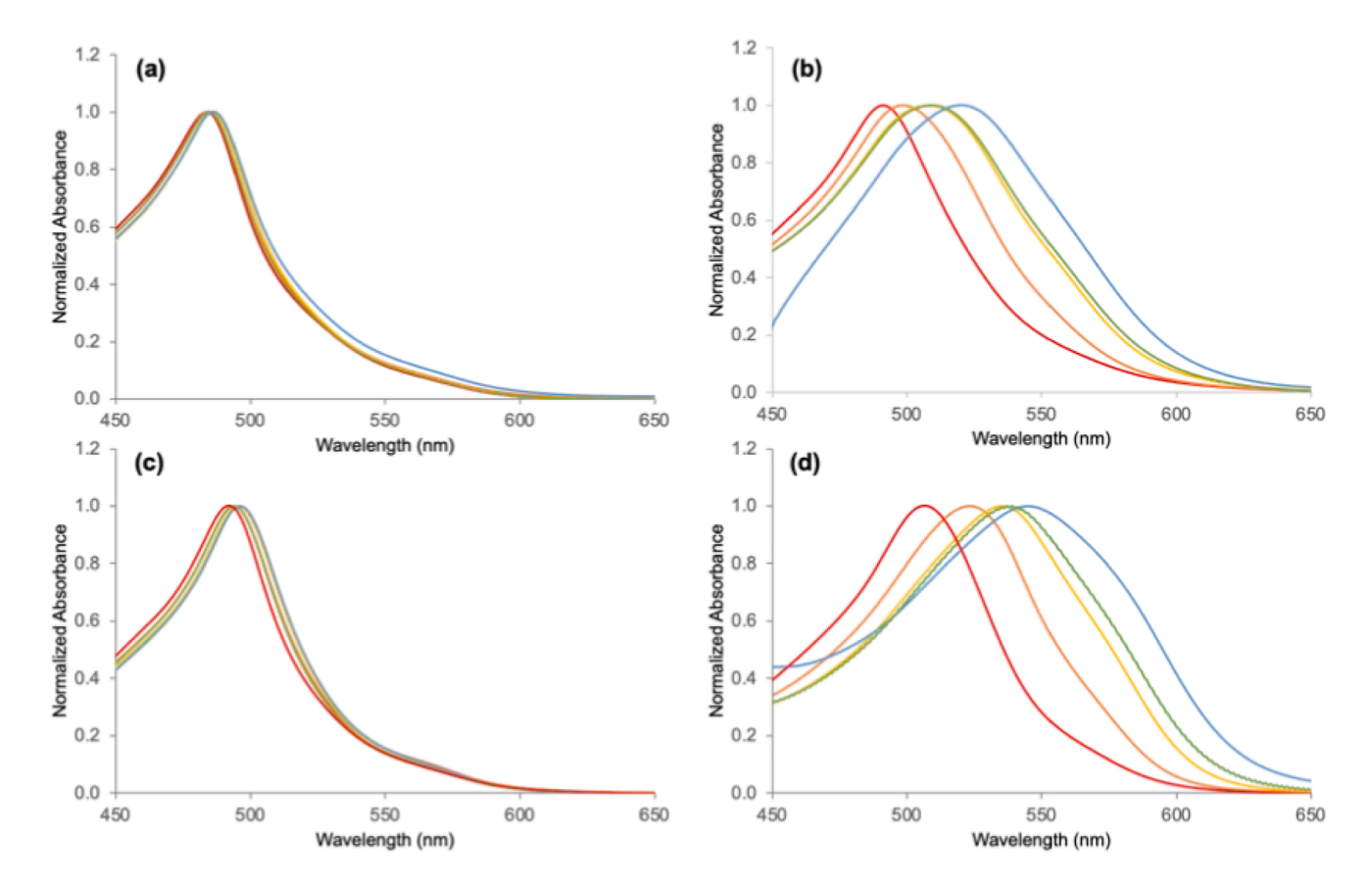


Fig. 5. Normalized UV/Visible absorbance spectra of (a)  $[Ru(tpy)(tpyPhOH)]^{2+}$ , (b)  $[Ru^{II}(tpy)(tpyPhO^{\circ})]^{+}$ , (c)  $[Ru(tpyPhOH)_2]^{2+}$ , and (d)  $[Ru^{II}(tpyPhO^{\circ})_2]$  in varying solvents and 5% DMSO. Solvents are red (-) = water, orange (-) = methanol, yellow (-) = ethanol, green (-) = acetonitrile, blue (-) = acetone.

**Table 3**Wavelength maxima of Ru complexes in different protonation states and solvents.

	Dieelectric	wavelength maxima (	wavelength maxima (nm)				
	Constant	[Ru(tpy)(tpyPhOH)] <sup>2</sup>	[Ru(tpy)(tpyPhOH)] <sup>2+</sup>		[Ru(tpyPhOH) <sub>2</sub> ] <sup>2+</sup>		
		protonated	deprotonated	protonated	deprotonated		
water	78.52	483	498	493	511		
methanol	32.6	485	499	494	524		
ethanol	24.6	486	508	496	535		
acetonitrile	36.64	485	509	494	537		
acetone	21.01	486	518	496	548		

All solvents also contained 5% DMSO to help increase solubility and ensure consistency.

the red shift in wavelength maxima. However, hydrogen bonding solvents result in an overall smaller red shift. We have previously observed these effects with the  $[Ru(bpy)_2(4,4'bpy(OH)_2)]^{2+}$  complex, where the hydroxyl groups are directly attached to the bipyridine ring [23]. In the deprotonated complex, [Ru<sup>II</sup>(tpy)(tpyPhO<sup>-</sup>)]<sup>+</sup>, the peak maxima shifts  $100~{\rm cm}^{-1}$  in methanol and  $400~{\rm cm}^{-1}$  in ethanol as compared to water, while the peak maxima shift 500 cm<sup>-1</sup> in acetonitrile and 800 cm<sup>-1</sup> in acetone in non-hydrogen bonding solvents. Hydrogen bonding stabilization of the deprotonated phenoxide is attributed to the less dramatic maxima shift in wavelength maxima, which results in more phenol-like character. Similar effects are observed for the deprotonated [Ru<sup>II</sup>(tpy-PhO<sup>-</sup>)<sub>2</sub>] complex, but larger due to the second tpyPhO<sup>-</sup> ligand, with peak maxima shifts in hydrogen bonding solvent of 500 cm<sup>-1</sup> in methanol and 800 cm<sup>-1</sup> in ethanol, as compared to water. The peak maxima shift is also more dramatic in acetonitrile and acetone with shifts of 900  ${\rm cm}^{-1}$ and 1400 cm<sup>-1</sup>, respectively, as compared to water.

The wavelength maxima shifts also scale as a function of dielectric constant and hydrogen bonding ability of the solvent when comparing the protonated and deprotonated forms of the complexes. For the [Ru (tpy)(tpyPhOH)]^2+complex, the peak maxima red shifts when deprotonated 600 cm $^{-1}$  in water,  $600~{\rm cm}^{-1}$  in methanol, and 900 cm $^{-1}$  in ethanol. When moving to non-hydrogen bonding solvents, these red shifts upon deprotonation increase to  $1000~{\rm cm}^{-1}$  in acetonitrile and  $1300~{\rm cm}^{-1}$  in acetone. Similar, but larger, red shifts are observed in the deprotonation of the [Ru(tpyPhOH)2]^2+ complex due to additional charge neutralization as a result of the second tpyPhOH ligand. For hydrogen bonding solvents, the red shift between protonated and deprotonated forms of the complex are  $700~{\rm cm}^{-1}$  in water,  $1100~{\rm cm}^{-1}$  in methanol, and  $1500~{\rm cm}^{-1}$  in ethanol. For non-hydrogen bonding solvents, these red shifts are  $1600~{\rm cm}^{-1}$  in acetonitrile and  $2000~{\rm cm}^{-1}$  in ethanol.

#### 3.4. Computational analysis of electronic transitions

Theoretical calculations were carried out on both protonated and deprotonated forms of the  $[Ru(tpy)(tpyPhOH)]^{2+}$  and  $[Ru(tpyPhOH)_2]^{2+}$  complexes using water as the PCM solvent to gain insight

Table 4 Calculated electronic transitions of  $[Ru(tpy)(tpyPhOH)]^{2+}$  and  $[Ru^{II}(tpy)(tpyPhO^-)]^+$  in PCM water.

Complex	$\lambda_{max}$ (nm)	Oscillator strength	Transition type
Protonated	519	0.124	$MML \rightarrow L_{tpvPhOH}$
	500	0.058	$M \rightarrow L_{tpy,tpyPhOH}$
	482	0.206	$M \rightarrow L_{tpy,tpyPhOH}$
	482	0.056	$M \rightarrow L_{tpy,tpyPhOH}$
Deprotonated	770	0.250	$MML1 \rightarrow L_{tpyPhO}$
	542	0.077	$MML1 \rightarrow L_{tpvPhO}$
	471	0.144	$M \rightarrow L_{tpy}$
	466	0.053	$MML2 \rightarrow L_{tpy,tpyPhO}$

MML, MML1, MML2 = Mixed metal-ligand orbitals depicted in Fig. 6. M = Orbital centralized on the metal.  $L_{tpy}$ ,  $L_{tpyPhOH}$ ,  $L_{tpyPhO}$ . = Empty ligand orbitals.

into the nature of the transitions. The protonated [Ru(tpy)(tpyPhOH)]<sup>2+</sup> complex has four low energy transitions, Table 4. The lowest energy transition predicted at 519 nm is from a mixed metal-ligand orbital (MML, Fig. 6) to the phenol-substituted terpyridine ligand. The other three transitions occur from metal centered orbitals to ligand orbitals on both the unsubstituted and phenol-substituted terpyridine ligands. Lower energy absorbances are predicted upon deprotonation at 770 nm and 542 nm associated with transitions from a mixed metal-ligand orbital (MML1, Fig. 6) to a ligand orbital on the deprotonated phenoxide-substituted terpyridine ligand. The lower energy absorbance shift from 519 nm in the protonated form to 542 nm in the deprotonated complex ( $\Delta 800 \text{ cm}^{-1}$ ) is similar to that observed in the experimental UV/Visible absorbance spectrum in water where the wavelength maximum shifts from 483 nm to 498 nm ( $\Delta 600 \text{ cm}^{-1}$ ). The calculated lowest energy transition at 770 nm is not observed experimentally. This new low-energy transition is due to destabalization of the highest occupied orbitals, which are mixed metal-ligand in nature, by the new lone pair formed on oxygen through deprotonation. Lack of an observed transition could be due to experimental factors (e.g., vibrational Frank-Condon), but there is also a possibility that the simple one-electron excitation TDDFT model is not adequate for quantitative prediction of such low-energy transitions. There are also two additional transitions predicted at 471 nm from a metal-centered orbital to the unsubstituted terpyridine ligand and at 466 nm from a mixed metal-ligand orbital (MML2, Fig. 6) to an orbital on both the unsubstituted and phenoxysubstituted terpyridine ligands.

For the [Ru(tpyPhOH)<sub>2</sub>]<sup>2+</sup> complex in both the protonated and deprotonated state, several new transitions are observed to unoccupied mixed metal–ligand orbitals, Fig. 7, that are not observed with the [Ru (tpy)(tpyPhOH)]<sup>2+</sup> complex. Two transitions are present at 530 nm and 494 nm, Table 5, in the protonated complex. The transition at 530 nm originates from a mixed metal–ligand orbital (MML3, Fig. 6) to an empty mixed metal–ligand orbital (ML<sub>tpyPhOH</sub>, Fig. 7). The transition at 494 nm is a standard metal to ligand charge transfer from the metal center to the empty ligand orbitals. Notably, in comparing the protonated forms of both complexes, the experimental  $\lambda_{max}$  of the protonated complexes in aqueous solution shifts 400 cm<sup>-1</sup> from [Ru(tpy)(tpyPhOH)]<sup>2+</sup> (483 nm) to [Ru(tpyPhOH)<sub>2</sub>]<sup>2+</sup> (493 nm). This same 400 cm<sup>-1</sup> shift is predicted in the computational data with [Ru(tpy)(tpyPhOH)]<sup>2+</sup> predicted at 519 nm and [Ru(tpyPhOH)<sub>2</sub>]<sup>2+</sup> predicted at 530 nm.

Four electronic transitions are predicted upon deprotonating the [Ru (tpyPhOH)<sub>2</sub>]<sup>2+</sup> complex to [Ru(tpyO´)<sub>2</sub>]. The two lowest energy transitions at 789 nm and 545 nm, occur from two degenerate mixed metal–ligand orbitals (MML4 and MML5, Fig. 6). The transition predicted at 789 nm occurs from MML4 and MML5 to two degenerate unoccupied mixed metal–ligand orbitals (1ML<sub>tpyPhO</sub>. and 2ML<sub>tpyPhO</sub>., Fig. 7). Similar to what is observed for the deprotonated [Ru<sup>II</sup>(tpy)(tpyPhO˙)]<sup>+</sup> complex, the low energy transition is not observed experimentally, and is attributed to the same phenomenon mentioned previously; the destabilization of the highest occupied mixed metal–ligand orbitals by the new lone pair orbitals on the deprotonated oxygens. The 545 nm transition occurs from the degenerate MML4 and MML5 orbitals to a ligand orbital. This transition is shifted 500 cm<sup>-1</sup> when compared to the

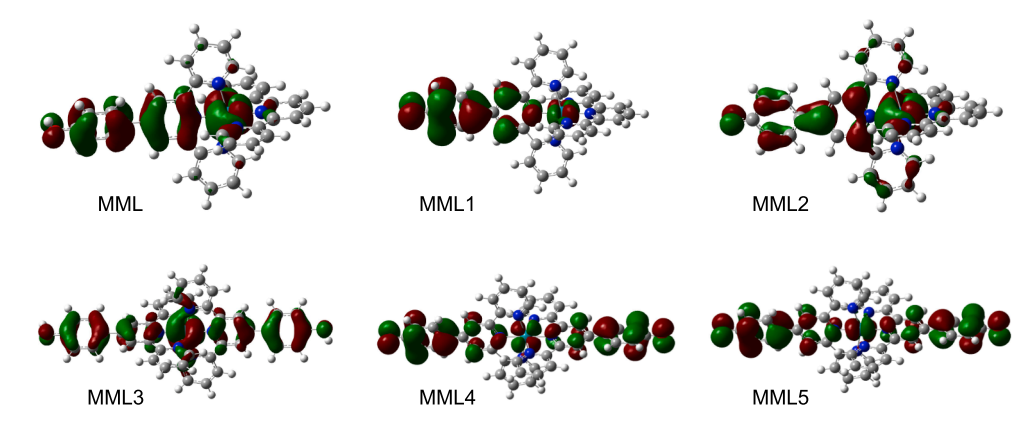


Fig. 6. Occupied mixed metal-ligand orbitals involved in electronic transitions.  $MML = [Ru(tpy)(tpyPhOH)]^{2+}$ , MML1 and  $MML2 = [Ru^{II}(tpy)(tpyPhO^{-})]^{+}$ , MML3 =  $[Ru(tpyPhOH)_{2}]^{2+}$ , MML4 and  $MML5 = [Ru^{II}(tpyPhO^{-})_{2}]$ . MML4 and MML5 are degenerate orbitals.

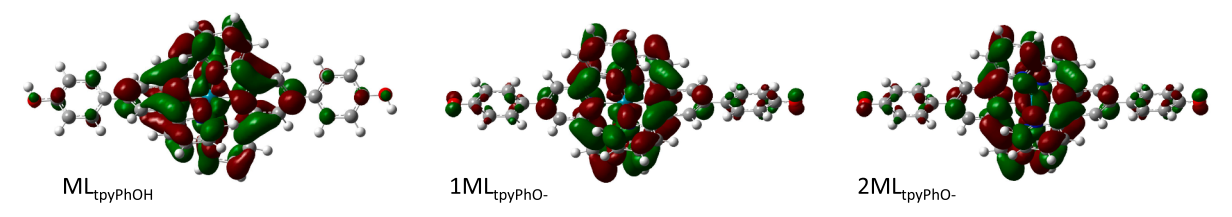


Fig. 7. Unoccupied mixed metal–ligand orbitals involved in electronic transitions.  $ML_{tpyPhOH} = [Ru(tpyPhOH)_2]^{2+}$ ,  $1ML_{tpyPhO}$  and  $2ML_{tpyPhO}$  and  $2ML_{tpyPhO}$  are degenerate orbitals.

Table 5 Calculated electronic transitions of  $[Ru(tpyPhOH)_2]^{2+}$  and  $[Ru^{II}(tpyPhO^-)_2]$  in PCM water.

Complex	$\lambda_{max}$ (nm)	Oscillator strength	Transition type
Protonated	530 494	0.327 0.323	$\begin{aligned} MML3 &\rightarrow ML_{tpyPhOH} \\ M &\rightarrow L_{tpyPhOH} \end{aligned}$
Deprotonated	789 545 507 474	0.515 0.144 0.066 0.103	$\begin{split} & \text{MML4,5} \rightarrow 1,2 \text{ML}_{tpyPhO}.\\ & \text{MML4,5} \rightarrow L_{tpyPhO}.\\ & \text{M} \rightarrow L_{tpyPhO}.\\ & \text{M} \rightarrow 1,2 \text{ML}_{tpyPhO}. \end{split}$

MML3, MML4, MML5 = Mixed metal-ligand orbitals depicted in Fig. 6. M = Orbital centralized on the metal.  $ML_{tpyPhOH}$ ,  $1ML_{tpyPhO-}$ ,  $2ML_{tpyPhO-}$  = Empty mixed metal-ligand orbitals depicted in Fig. 7.  $L_{tpyPhOH}$ ,  $L_{tpyPhO-}$  = Empty ligand orbitals.

calculated 530 nm transition of the protonated form. The comparative experimental UV/Visible spectra in water give a 700 cm $^{-1}$  shift (from 493 nm to 511 nm) from the protonated to deprotonated form. The next electronic transition at 507 nm is a typical metal to ligand charge transfer transition, while the 474 nm transition is a metal to the two degenerate unoccupied mixed metal–ligand orbitals (1ML $_{\rm typPhO}$ - and 2ML $_{\rm typPhO}$ -, Fig. 7).

### 3.5. Electrochemistry

Electrochemical analysis of [Ru(tpy)(tpyPhOH)]Cl $_2$  was performed in aqueous Britton-Robinson buffer to determine the impact of pH on the redox potentials of the complex. 5% DMSO was added to aid solubility but aqueous broad cyclic voltammetry (CV) waveshapes on glassy carbon electrodes prevented the reliable quantitative potential determination, which we attribute to poor electron transfer kinetics. Alternatively, differential pulse voltammetry (DPV) did allow the redox potentials to be determined for the complex. A single redox process is observed at  $E_{\rm red} = 0.72$  V vs. Ag/AgCl under acidic conditions (pH < 6).

As the pH increases, two redox processes evolve, one that is pH dependent with  $E_{\rm red}=0.58~V$  vs. Ag/AgCl at pH >10 and a second at  $E_{\rm red}=0.75~V$  vs. Ag/AgCl that is pH independent, Fig. 8. The ability for the complex to lose the proton results in greater ease of oxidation, and the ability to readily lose a second electron. Attempts to study the [Ru (tpyPhOH)\_2]Cl\_2 complex in aqueous solution were largely unsuccessful due poor solubility, as attempts to increase its aqueous solubility by adding DMSO failed and prevented electrochemical analysis.

CV analysis of  $[Ru(tpy)(tpyPhOH)]^{2+}$  was pursued in acetonitrile, Fig. 9a (black line), with 0.1 M TBAPF<sub>6</sub> as supporting electrolyte, and two overlapping oxidations appear. Repeating the experiment with 0.1 M hexafluorophosphoric acid results in a single reversible redox process at 0.85 V vs.  $Fc^{+/0}$ , Fig. 9a (red line), which is between the reduction potential of  $[Ru(tpy)_2]^{2+}$  (0.89 V vs.  $Fc^{+/0}$ ) and  $[Ru(tpy)(tpyOH)]^{2+}$  (0.79 V vs.  $Fc^{+/0}$ ). This indicates that the phenol-moiety is mostly behaving as an electron-withdrawing substituent "phenyl" substituent rather than an electron-donating hydroxy-substituent, as is the case in  $[Ru(tpy)(tpyOH)]^{2+}$  [24]. Thus, the phenyl spacer is serving to dampen or decouple the hydroxy functionality from the metal center.

An irreversible oxidation that appears at 0.83 V vs  $Fc^{+/0}$  followed by a reversible redox process at 0.91 V vs.  $Fc^{+/0}$  when water is added to the acetonitrile solution, Fig. 9a (blue line). Importantly, addition of water to the acetonitrile solution shifts the oxidation to lower-potentials in accordance with a chemical step (e.g. proton transfer to water) in an electrochemically reversible, chemically reversible mechanism E<sub>r</sub>C<sub>r</sub> [59], followed by another electrochemical step, following an ECE mechanism presented in equations 1–3. Additionally, proton loss to the solvent is disfavored under acidic conditions and results in a single reversible redox process according to equation 2 without undergoing further redox processes. While the origin of the second couple is unclear, we hypothesize that oxidation of a semiquinone-like radical occurs after proton loss according to equation 3. Aqueous DPV data is consistent with the proposed mechanism and justifies why the second couple, revealed at basic pHs, is pH independent while the first redox couple displays a pH dependence depicted in Fig. 8. Furthermore, CV simulations, using Gamry's DigiElch Electrochemical Simulation Software, are in good

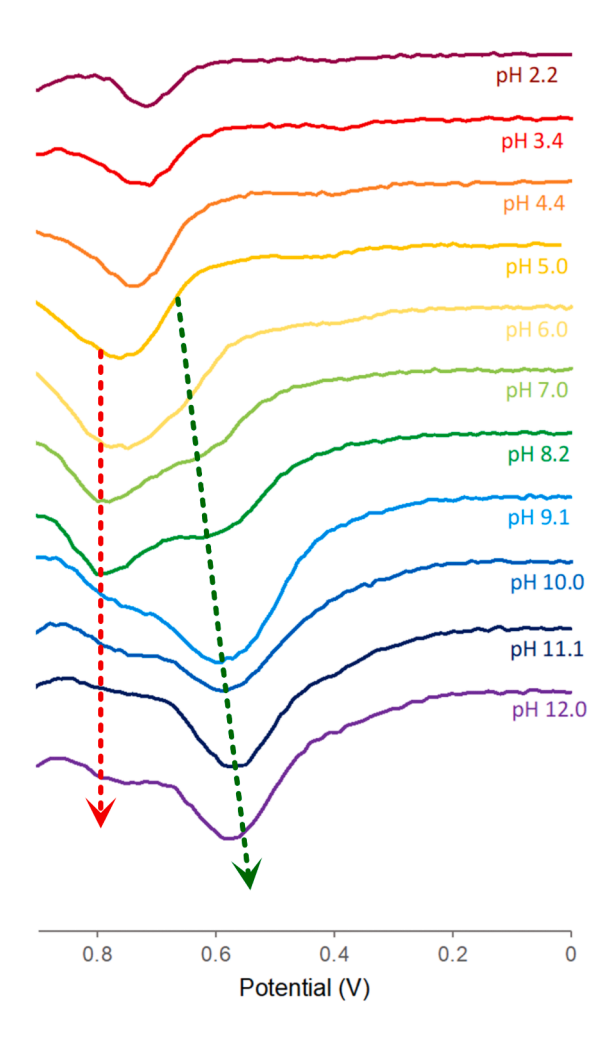


**Fig. 8.** DPV of [Ru(tpy)(tpyPhOH)]Cl<sub>2</sub> in Britton Robinson buffer with 5% DMSO. The green dashed line depicts the pH dependence of one couple while the red dashed line indicates a second couple's pH independence.

agreement with the proposed ECE mechanism (see Figure S31).

The resonance stabilization depicted in equation 4, where the semiquinone-like radical formally reduces the Ru, explains why the two couples are within 0.1 V of one another rather than larger potentials associated with unstabilized sequential oxidation events. Further oxidation of  $[Ru^{II}(tpy)(tpyPhOH)]^{3+}$  in strongly acidic solutions would require another metal centered oxidation to  $Ru^{IV}$  state at much more anodic potentials as a semiquinone-type oxidation is inaccessible in its protonated state. Quinones, semiquinones, and hydroquinones are known for their rich redox chemistry, even displaying rich electrochemical behavior in bimetallic ruthenium complexes [60-62]. The first irreversible oxidation also loosely resembles irreversible oxidation of phenols due to proton loss to solvent previously observed [63].

$$[Ru^{II}(tpy)(tpyPhOH)]^{2+} \rightleftharpoons [Ru^{III}(tpy)(tpyPhOH)]^{3+} + e^{-}E_{p,a} = 0.83 \text{ V}$$
 (1)

$$[Ru^{III}(tpy)(tpyPhOH)]^{3+} + B \rightleftharpoons [Ru^{III}(tpy)(tpyPhO^{-})]^{2+} + HB^{+}$$
 (2)

$$[Ru^{III}(tpy)(tpyPhO-)]^{2+} \Rightarrow [Ru^{III}(tpy)(tpyPhO^{\bullet})]^{3+} + e^{-}E_{1/2} = 0.91 \text{ V}$$
 (3)

$$[Ru^{III}(tpy)(tpyPhO^{\bullet})]^{3+} \leftrightarrow [Ru^{IV}(tpy)(tpyPh = O)]^{3+}$$
(4)

[Ru(tpyPhOH)<sub>2</sub>](PF<sub>6</sub>)<sub>2</sub> appears to behave similarly to [Ru(tpy)(tpy-PhOH)](PF<sub>6</sub>)<sub>2</sub> in acetonitrile, Fig. 9b (black line), upon initial analysis. First, two redox couples resolve upon the addition of water to an acetonitrile solution, Fig. 9b (blue line). One irreversible oxidation at 0.80 V vs. Fc<sup>+/0</sup> is followed by a reversible redox process at 0.90 V vs.  $\mathrm{Fc}^{+/0}$  and imply that they were overlapping prior to the addition of a solvent capable of accepting a lost proton. Next, a single reversible redox process at 0.88 V vs.  $Fc^{+/0}$  is observed when hexafluorophosphoric acid is added to a 0.1 M TBAPF<sub>6</sub> acetonitrile solution, Fig. 9b (red line). However, careful analysis of scan rate dependent scans in acetonitrile with 0.1 M HPF<sub>6</sub> indicates the presence of two reversible couples of similar potentials (see Figure S29). We attribute this first couple to oxidation of ruthenium without the loss of a proton (eqn. 5), similar to that of [Ru<sup>II</sup>(tpy)(tpyPhOH)]<sup>2+</sup> (eqn. 4). We speculate that the second oxidation occurs following a coupled electron-proton transfer process that avoids charge buildup (eqn. 6).

$$[Ru^{II}(tpvPhOH)_2]^{2+} \rightleftharpoons [Ru^{III}(tpvPhOH)_2]^{3+} + e^{-}$$
(5)

$$[Ru^{III}(tpyPhOH)_2]^{3+} \rightleftharpoons [Ru^{IV}(tpyPhOH)(tpyPhO^{\bullet})]^{3+} + H^{+} + e^{-}$$
 (6)

We note that the redox couple,  $[Ru^{II}(tpyPhOH)_2]^{2+} \rightleftharpoons [Ru^{III}(tpyPhOH)_2]^{3+} + e^{-}$ , indicates  $[Ru^{II}(tpyPhOH)_2]^{2+}$  is more electron deficient than  $[Ru^{II}(tpy)(tpyPhOH)]^{2+}$  when considering its analogous couple (eqn. 2;  $E_{1/2} = 0.83$  V). This data further indicates that the

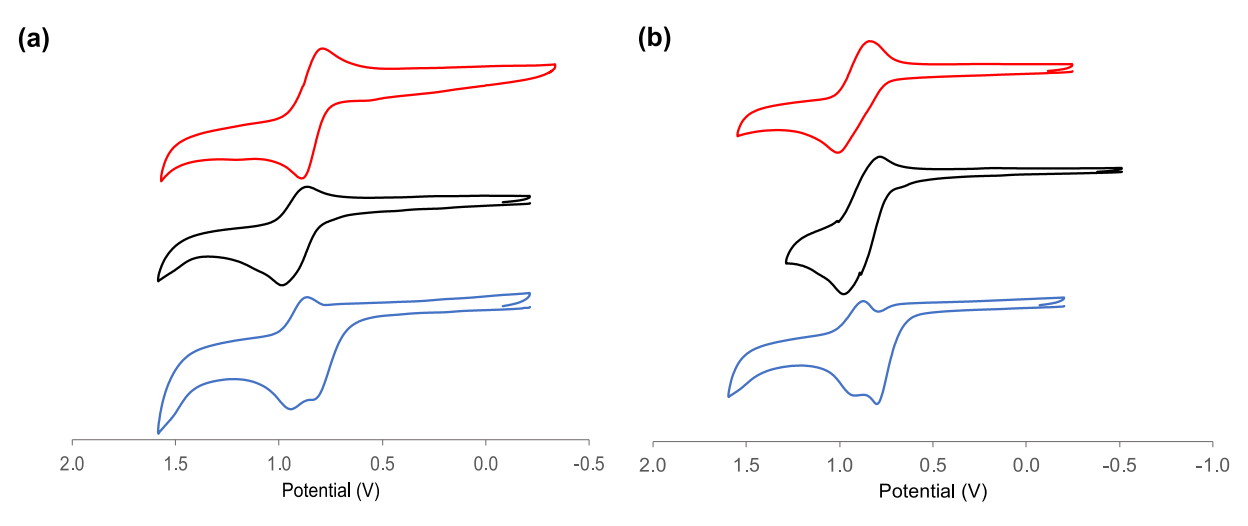


Fig. 9. Cyclic voltammograms of (a) 1.5 mM [Ru(tpy)(tpyPhOH)](PF<sub>6</sub>)<sub>2</sub> and (b) 1.5 mM [Ru(tpyPhOH)<sub>2</sub>](PF<sub>6</sub>)<sub>2</sub> in 0.1 M TBAPF<sub>6</sub> in red (-) = acetonitrile with 0.1 M HPF<sub>6</sub>, black (-) = acetonitrile, and blue (-) = acetonitrile with added water (~20 mM). Scans were collected at a rate of 200 mV/s and reported vs. Fc<sup>+/0</sup> as an internal standard. All CVs are first scans except for the red trace in (a) which is the fourth scan (See SI Figure S25).

phenol groups offer little electron-donation to the metal center and the 4'-substituent is primarily inductively withdrawing in nature. Conversely, the  $[Ru(tpyOH)_2]^{2+}$  complex  $(0.71\ V\ vs.\ Fc^{+/0})$ , is significantly more electron-donating than the  $[Ru(tpyPhOH)_2]^{2+}$  complex and behaves as expected with electron donor character when compared to  $[Ru(tpy)_2]^{2+}$   $(0.89\ V\ vs.\ Fc^{+/0})$  [24].

Unfortunately, attempts to fully deprotonate the complexes in acetonitrile when various concentrations of tetra-*n*-butyl ammonium hydroxide, TBAOH, was added to the electrochemistry solutions, resulted in poor quality voltammograms, likely due to combination of reduced solubility and base oxidation on the electrode.

#### 4. Conclusions

New complexes,  $[Ru(tpy)(tpyPhOH)](PF_6)_2$  and  $[Ru(tpyPhOH)_2]$   $(PF_6)_2$ , were synthesized and characterized by cyclic voltammetry, differential pulse voltammetry, UV–Vis spectroscopy, and single crystal X-ray crystallography to determine the impact that a phenyl spacer at the 4'-position of tpy has on electronic properties of the ruthenium system.

CV analysis in acetonitrile allowed for the characterization of both electrochemical and chemical steps that occur with the multi-step oxidations. The first oxidation is pH dependent and likely follows a PCET process, while the second oxidation is ligand centered and generates a semiquinone-like radical that can avoid the buildup of charge. At low pH only one redox event occurs due to the inaccessibility to a high energy electron, either metal centered or phenolic in origin. This data is consistent with CV simulations and aqueous DPV results. The relative redox potentials of the related homoleptic complexes discussed above  $PhOH)_2](PF_6)_2$ , where  $[Ru(tpyPhOH)_2](PF_6)_2$  is the most electron deficient. Crystallographic and computational modeling are in general agreement, although intermolecular interactions in the crystal structure play a role in twisting of the phenol-ring structure. When compared to [Ru(tpyOH)<sub>2</sub>](PF<sub>6</sub>)<sub>2</sub> it is noteworthy that the pK<sub>a</sub> is significantly greater (by over 3 pK<sub>2</sub> units) with the phenyl spacer.

Overall, these results indicate that the phenyl spacer is weakly coupled to the metal-center and primarily behaves as an electron withdrawing moiety in a homoleptic complex rather than when the hydroxy- group is directly attached to the 4'-position of terpyridine. However, the phenol-moiety does offer a mechanism to facilitate an additional oxidation of the complexes, where phenolate oxidation generates a semiquinone-like radical in conjugation with the metal.

#### CRediT authorship contribution statement

Katherine L. Moffa: Validation, Methodology, Formal analysis, Investigation, Writing – review & editing, Visualization. Claire N. Teahan: Investigation. Charlotte L. Montgomery: Investigation. Samantha L. Shepherd: Investigation. John C. Dickenson: Investigation. Kaitlyn R. Benson: Investigation. Mark Olsen: Investigation. Methodology. Walter J. Boyko: Investigation. Mark Bezpalko: Investigation, Formal analysis. W. Scott Kassel: Investigation. Timothy J. Dudley: Methodology, Formal analysis, Investigation, Visualization. Daniel P. Harrison: Conceptualization, Methodology, Formal analysis, Investigation, Writing – original draft, Writing – review & editing, Visualization, Supervision, Project administration, Funding acquisition. Jared J. Paul: Conceptualization, Methodology, Formal analysis, Investigation, Writing – original draft, Writing – review & editing, Visualization, Supervision, Project administration, Funding acquisition.

#### **Declaration of Competing Interest**

The authors declare that they have no known competing financial interests or personal relationships that could have appeared to influence the work reported in this paper.

#### Data availability

No data was used for the research described in the article.

#### Acknowledgements

Funding for this project comes from a grant from the National Science Foundation – Chemistry Structure, Dynamics & Mechanisms B (CHE-1900536). This work was also supported by Major Research Instrumentation grants from the National Science Foundation (CHE-1827930 and CHE-2018399). Support from the College of Liberal Arts and Sciences at Villanova University is gratefully acknowledged as is the support from the Virginia Military Institute's Grants-in-Aid of Research supply funds.

Appendix A. Supplementary data Infrared spectroscopy, 1H-NMR spectroscopy, electrochemistry, and UV/visible spectroscopy data, CV Simulation Parameters, XYZ coordinates for each computationally optimized structure. CIF files.

Supplementary data to this article can be found online at https://doi. org/10.1016/j.poly.2023.116582.

#### References

- D.R. Weinberg, C.J. Gagliardi, J.F. Hull, C.F. Murphy, C.A. Kent, B.C. Westlake, A. Paul, D.H. Ess, D.G. McCafferty, T.J. Meyer, Chem Rev 112 (2012) 4016–4093.
- [2] S. Hammes-Schiffer, Acc Chem Res 42 (2009) 1881-1889.
- [3] J.L. Dempsey, J.R. Winkler, H.B. Gray, Chem Rev 110 (2010) 7024-7039.
- [4] C. Costentin, Chem Rev 108 (2008) 2145-2179.
- [5] R.I. Cukier, D.G. Nocera, Annu Rev Phys Chem 49 (1998) 337-369.
- [6] J.M. Mayer, Annu Rev Phys Chem 55 (2004) 363-390.
- [7] M.H.V. Huynh, T.J. Meyer, Chem Rev 107 (2007) 5004–5064.
- [8] R. Tyburski, T. Liu, S.D. Glover, L. Hammarström, J. Am. Chem. Soc. 143 (2) (2021) 560–576.
- [9] J.W. Darcy, B. Koronkiewicz, G.A. Parada, J.M. Mayer, Acc. Chem. Res. 51 (10)
- [10] M.D. Karkas, O. Verho, E.V. Johnston, B. Akermark, Chem Rev 114 (2014) 11863–12001.
- [11] O.S. Wenger, Acc. Chem. Res. 46 (7) (2013) 1517–1526.
- [12] M. Brautigam, M. Wachtler, S. Rau, J. Popp, B. Dietzek, J Phys Chem C 116 (2012) 1274–1281.
- [13] M. Haga, M.M. Ali, H. Maegawa, K. Nozaki, A. Yoshimura, T. Ohno, Coord Chem Rev 132 (1994) 99–104.
- [14] M. Haga, M.M. Ali, S. Koseki, K. Fujimoto, A. Yoshimura, K. Nozaki, T. Ohno, K. Nakajima, D.J. Stufkens, Inorg Chem 35 (1996) 3335–3347.
- [15] Y. Miyazato, T. Wada, J.T. Muckerman, E. Fujita, K. Tanaka, Angew Chem Int Ed 46 (2007) 5728–5730.
- [16] S. Miyazaki, T. Kojima, J.M. Mayer, S. Fukuzumi, J Am Chem Soc 131 (2009) 11615–11624.
- [17] V.W. Manner, J.M. Mayer, J Am Chem Soc 131 (2009) 9874-9875.
- [18] S. Baitalik, S. Dutta, P. Biswas, U. Florke, E. Bothe, K. Nag, Eur J Inorg Chem (2010) 570–588.
- [19] S. Baitalik, U. Florke, K. Nag, J Chem Soc Dalton Trans (1999) 719–727.
- [20] P.J. Giordano, C.R. Bock, M.S. Wrighton, J Am Chem Soc 100 (1978) 6960–6965.
- J.M. Price, W. Xu, J.N. Demas, B.A. DeGraff, Anal Chem 70 (1998) 265–270.
   Thompson, A. M. W. C.; Smailes, M. C. C.; Jeffery, J. C.; Ward, M. D. Dalton Trans 1997, 737–744.
- [23] S. Klein, W.G. Dougherty, W.S. Kassel, T.J. Dudley, J. Paul, J. Inorg. Chem. 50 (2011) 2754–2763.
- [24] K.A. Maghacut, A.B. Wood, W.J. Boyko, T.J. Dudley, J.J. Paul, Polyhedron 67 (2014) 329–337.
- [25] M.J. Fuentes, R.J. Bognanno, W.G. Dougherty, W.J. Boyko, W.S. Kassel, T. J. Dudley, J.J. Paul, Dalton Trans 41 (40) (2012) 12514–12523.
- [26] E.J. Peterson, A.E. Kuhn, M.H. Roeder, N.A. Piro, W.S. Kassel, T.J. Dudley, J. J. Paul. Dalton Trans. 47 (2018) 4149-.
- [27] K.R. Benson, J. Stash, K.L. Moffa, R.H. Schmehl, T.J. Dudley, J.J. Paul, Polyhedron 205 (2021), 115300.
- [28] J. DePasquale, I. Nieto, L.E. Reuther, C.J. Herbst-Gervasoni, J.J. Paul, V. Mochalin, M. Zeller, C.M. Thomas, A.W. Addison, E.T. Papish, Inorg Chem 52 (16) (2013) 9175–9183.
- [29] K.T. Hufziger, F.S. Thowfeik, D.J. Charboneau, I. Nieto, W.G. Dougherty, W. S. Kassel, T.J. Dudley, E.J. Merino, E.T. Papish, J.J. Paul, J. Inorg. Biochem. 130 (1) (2014) 103–111
- [30] E. Amtmann, M. Zöller, H. Wesch, G. Schilling, Cancer Chemother, Pharmacol. 47 (6) (2001) 461–466.
- [31] Y. Gou, Y. Zhang, J. Qi, S. Chen, Z. Zhou, X. Wu, H. Liang, F. Yang, Oncotarget 7 (41) (2016) 67004–67019.

- [32] D.J. Charboneau, N.A. Piro, W.S. Kassel, T.J. Dudley, J.J. Paul, Polyhedron 91 (2015) 18–27.
- [33] J.C. Dickenson, M.E. Haley, J.T. Hyde, Z.M. Reid, T.J. Tarring, D.A. Iovan, D. P. Harrison, Inorg. Chem. 60 (13) (2021) 9956–9969.
- [34] B.P. Sullivan, J.M. Calvert, T.J. Meyer, Inorg Chem 19 (1980) 1404-1407.
- [35] D.-W. Yoo, S.K. Yoo, C. Kim, J. Lee, J. Chem. Soc. Dalton Trans. 21 (2002) 3931–3932.
- [36] D.C. Marelius, S. Bhagan, D.J. Charboneau, K.M. Schroeder, J.M. Kamdar, A. R. McGettigan, B.J. Freeman, C.E. Moore, A.L. Rheingold, A.L. Cooksy, D.K. Smith, J.J. Paul, E.T. Papish, D.B. Grotjahn, Eur. J. Inorg. Chem. 2014 (4) (2014) 676–689.
- [37] APEX II. 2009.
- [38] A. Altomare, G. Cascarano, C. Giacovazzo, A. Guagliardi, M.C. Burla, G. Polidori, M. Camalli, J. Appl. Crystallogr. 27 (3) (1994).
- [39] P.W. Betteridge, J.R. Carruthers, R.I. Cooper, K. Prout, D.J. Watkin, J. Appl. Crystallogr. 36 (6) (2003).
- [40] R.I. Cooper, A.L. Thompson, D.J. Watkin, J. Appl. Crystallogr. 43 (5) (2010)
- [41] O.V. Dolomanov, L.J. Bourhis, R.J. Gildea, J.A.K. Howard, H. Puschmann, J. Appl. Crystallogr. 42 (2) (2009) 339–341.
- [42] G.M. Sheldrick, Acta Crystallogr, Sect. Found. Adv. 71 (1) (2015) 3-8.
- [43] G.J. Shugar, R.S. Bauman, R. Shugar, L. Bauman, Chemical Technicians' Ready Reference Handbook, 2nd Ed, McGraw-Hill Book Company, New York, NY, 1981.
- [44] Frisch, M. J.; Trucks, G. W.; Schlegel, H. B.; Scuseria, G. E.; Robb, M. A.; Cheeseman, J. R.; Scalmani, G.; Barone, V.; Mennucci, B.; Petersson, G. A.; Nakatsuji, H.; Caricato, M.; Li, X.; Hratchian, H. P.; Izmaylov, A. F.; Bloino, J.; Zheng, G.; Sonnenberg, J. L.; Hada, M.; Ehara, M.; Toyota, K.; Fukuda, R.; Hasegawa, J.; Ishida, M.; Nakajima, T.; Honda, Y.; Kitao, O.; Nakai, H.; Vreven, T.; Montgomery Jr., J. A.; Peralta, J. E.; Ogliaro, G.; M., B.; Heyd, J. J.; Brothers, E.; Kudin, K. N.; Staroverov, V. N.; Kobayashi, R.; Normand, J.; Raghavachari, K.; Rendell, A.; Burant, J. C.; Iyengar, S. S.; Tomasi, J.; Cossi, M.; Rega, N.; Millam, J. M.; Klene, M.; Knox, J. E.; Cross, J. B.; Bakken, V.; Adamo, C.; Jaramillo, J.; Gomperts, R.; Stratmann, R. E.; Yazvev, O.; Austin, A. J.; Cammi, R.; Pomelli, C.;

Ochterski, J. W.; Martin, R. L.; Morokuma, K.; Zakrzewski, V. G.; Voth, G. A.; Salvador, P.; Dannenberg, J. J.; Dapprich, S.; Daniels, A. D.; Farkas, O.; Foresman, J. B.; Ortiz, J. V.; Cioslowski, J.; Fox, D. J. Gaussian 09, Revision E. 01, 2009.

Polyhedron 244 (2023) 116582

- [45] M.L. Scudder, D.C. Craig, H.A. Goodwin, Cryst Eng Comm 7 (2005) 642-649.
- [46] J. McMurtrie, I. Dance, Cryst Eng Comm 7 (2005) 230-236.
- [47] F. Darabi, H. Hadadzadeh, J. Simpson, A. Shahpiri, New J. Chem. 40 (11) (2016) 9081–9097.
- [48] P. Zhou, L. Huang, Y. Zhang, X. Xue, Y. Zhou, Z.J. Ma, Photochem. Photobiol. Chem. 358 (2018) 17–25.
- [49] C.J. Janiak, Chem. Soc. Dalton Trans. 21 (2000) 3885-3896.
- [50] H. Iranmanesh, K.S.A. Arachchige, W.A. Donald, N. Kyriacou, C. Shen, J.R. Price, J. E. Beves, Aust. J. Chem. 70 (5) (2017) 529–537.
- [51] J. McMurtrie, I. Dance, CrstEngComm 11 (6) (2009) 1141.
- [52] E.C. Constable, C.E. Housecroft, E.A. Medlycott, M. Neuburger, F. Reinders, S. Reymann, S. Schaffner, Inorg. Chem. Commun. 11 (7) (2008) 805–808.
- [53] G.D. Will, G.J. Wilson, Inorg Chim Acta 363 (2010) 1627-1638.
- [54] L.E.V. Salgado, C. Vargas-Hernández, Am. J. Anal. Chem. 5 (17) (2014) 1290–1301.
- [55] M.D. Liptak, K.C. Gross, P.G. Seybold, S. Feldgus, G.C. Shields, J. Am. Chem. Soc. 124 (22) (2002) 6421–6427.
- [56] R. Casasnovas, J. Frau, J. Ortega-Castro, A. Salvà, J. Donoso, F. Muñoz, J. Mol. Struct. THEOCHEM 912 (1) (2009) 5–12.
- [57] CRC Handbook of Chemistry and Physics, 91st ed.; Haynes, W. M., Ed.; CRC Press: Boca Raton, 2011.
- [58] E.M. Kober, B.P. Sullivan, T.J. Meyer, Inorg Chem 23 (1984) 2098-2104.
- [59] A.J. Bard, L.R. Faulkner, Electrochemical Methods: Fundamentals Applications, 3rd ed., Henry S, John Wiley and Sons Ltd, 2022.
- [60] S. Maji, B. Sarkar, S.M. Mobin, J. Fiedler, F.A. Urbanos, R. Jimenez-Aparicio, W. Kaim, G.K. Lahiri, Inorg. Chem. 47 (12) (2008) 5204–5211.
- [61] B. Huskinson, M.P. Marshak, C. Suh, S. Er, M.R. Gerhardt, C.J. Galvin, X. Chen, A. Aspuru-Guzik, R.G. Gordon, M.J. Aziz, Nature 505 (7482) (2014) 195–198.
- [62] P. Symons, Curr. Opin. Electrochem. 29 (2021), 100759.
- [63] M. Kuss-Petermann, O.S. Wenger, J Phys Chem A 117 (28) (2013) 5726–5733.